ACS APPLIED POLYMER MATERIALS

pubs.acs.org/acsapm

Article

Poly(ethylene oxide)-Based Electrolytes for Solid-State Potassium Metal Batteries with a Prussian Blue Positive Electrode

Anna D. Khudyshkina, Polina A. Morozova, Andreas J. Butzelaar, Maxi Hoffmann, Manfred Wilhelm, Patrick Theato, Stanislav S. Fedotov, and Fabian Jeschull*

Cite This: https://doi.org/10.1021/acsapm.2c00014

Read Online

ACCESS | Metrics & More | Article Recommendations | Supporting Information

ABSTRACT: Potassium-ion batteries are an emerging post-lithium technology that are considered ecologically and economically benign in terms of raw materials' abundance and cost. Conventional cell configurations employ flammable liquid electrolytes that impose safety concerns, as well as considerable degrees of irreversible side reactions at the reactive electrode interfaces (especially against potassium metal), resulting in a rapid capacity fade. While being inherently safer, solid polymer electrolytes may present a solution to capacity losses owing to their broad electrochemical stability window. Herein, we present for the first time a stable solid-state potassium battery composed of a potassium metal negative electrode, a Prussian blue analogue $K_2Fe[Fe(CN)_6]$ positive electrode, and a poly(ethylene oxide)-potassium bis(trifluoromethanesulfonyl)imide polymer electrolyte. At an elevated operating temperature of 55 °C, the solid-state battery achieved a superior capacity retention of 90% over 50 cycles in direct comparison to a conventional carbonate-based liquid electrolyte operated at ambient temperature with a capacity retention of only 66% over the same cycle number interval.

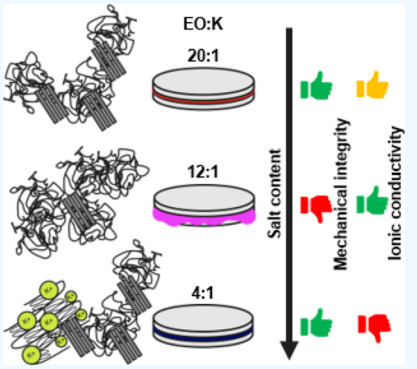

KEYWORDS: *potassium battery, solid polymer electrolytes, SPEs, polyethylene oxide, PEO, KTFSI, Prussian blue analogue, PBA*

1. INTRODUCTION

Potassium-ion batteries (PIBs) are a growing post-lithium battery technology that show advantages in terms of potassium crustal abundance leading to potentially lower material costs, which enable large-scale stationary energy storage applications.[1−3] PIBs are anticipated to approach or even exceed specific energies of most currently developed sodium-ion batteries, despite the fact that the larger atomic mass and cationic radius of potassium generally result in smaller volumetric and gravimetric capacities.[4] These shortcomings are often compensated by higher electrode potentials of commonly used cathode materials based on iron, manganese, or vanadium [e.g., Prussian blue analogues (PBAs) $K_2M[Fe(CN)_6]$ (M = Fe, Mn, etc.) or polyanionic compounds, such as $KVOPO_4$ and $KVPO_4F$],[5−8] with the potential to boost the PIB cell voltage over 4 V.[9,10] However, using high-voltage materials puts high demands on the anodic stability of the electrolyte, as previously shown by Kim et al.[11]

On the anode side, the potential of the cell could be further broadened, when potassium metal is used instead of composite electrodes, for example, from graphite[12,13] or antimony.[14] This raises safety concerns due to the significantly increased reactivity of potassium as compared to that of lithium or sodium.[1] Moreover, in conventional organic liquid electrolytes (LEs), recurring irreversible electrolyte degradation reactions at the solid electrolyte interfaces (SEIs) are quite severe, causing growing interface resistances,[15] dendrite growth, and fast electrolyte consumption, culminating in a rapid capacity fade.

To overcome these issues, LEs can be replaced by solid polymer electrolytes (SPEs) that are beneficial in terms of mechanical and electrochemical stability due to their inherent inertness and thermotolerance.[16−19] In fact, in a previous study, Fei et al.[20] demonstrated improved capacity retention and Coulombic efficiencies (CEs) over a LE system of an anode half-cell when a solid poly(ethylene oxide) (PEO)-based electrolyte is employed. The same authors received similar promising results with an organic cathode with an average potential of 2.3 V vs K^+/K (on discharge).[10] In the context of SPEs, PEO is the most studied polymer host for SPE application in both lithium and sodium batteries[19] for its ability to dissolve high amounts of conductive salt, its low glass transition temperature ($T_g \approx -60$ °C),[19] and its broad electrochemical stability window.[21,22] For potassium batteries, SPEs, in general, and PEO-based SPEs, in particular, have so far received barely any attention. This is surprising, considering that many known shortcomings of SPEs that limit ion

Received: January 9, 2022
Accepted: February 25, 2022

transport in the polymer matrix are reduced with increasing cation size.[23] Specifically, the strong polydentate coordination between ethylene oxide units and the cation, the dissociation energy of the conducting salt, ion pairing effects, and the insufficient segmental motion of polymer chains below the melting temperature have hampered fast ionic transport in the past.[19]

Potassium salts generally exhibit lower dissociation energies and are less tightly bound to the monomer units of PEO and are two parameters that potentially facilitate K^+ transport within the polymer host.[23,24] To date, detailed studies on the most relevant electrolyte salt in this field, potassium bis-(trifluoromethane sulfonyl)imide (KTFSI), have not been carried out.[25] PEO-KTFSI blends place an important performance reference for future works and, as will be shown herein, are a relevant class to solid-state potassium batteries themselves.

In this work, we provide, for the first time, a detailed analysis of the thermal, rheological, and electrochemical properties of PEO-KTFSI formulations. Furthermore, we have identified several promising candidates providing both high ionic conductivities and mechanical stability within the relevant temperature range between 0 and 65 °C that could be employed as SPEs in potassium batteries. As a positive electrode, potassium iron hexacyanoferrate ($K_2Fe[Fe(CN)_6]$) was synthesized as a reliable electrode material with high capacity retention and high average electrode potential. The solid-state cell configuration comprising a K-metal anode, a PEO-KTFSI solid electrolyte, and a $K_2Fe[Fe(CN)_6]$ cathode with an average voltage of around 3.6 V (on discharge) demonstrated superior capacity retention and CE in comparison to a corresponding LE-cell, thus representing a competitive system to current state-of-the-art LE configurations.[4]

2. EXPERIMENTAL SECTION

2.1. Polymer Electrolyte Preparation. PEO (average M_v = 5,000,000, Sigma-Aldrich, lot # MKBR8472V) and KTFSI (99.5%, Solvionic) were dried at 110 °C for 12 h under vacuum (10^{-3} mbar) and transferred to the Ar-filled glovebox, where all following procedures were carried out under an inert atmosphere (H_2O < 0.1 ppm, O_2 < 0.1 ppm). The predefined amounts of the polymer and KTFSI corresponding to the molar ratios of ethylene oxide (EO):K = 20:1, 16:1, 12:1, 8:1, and 4:1 were homogeneously dissolved in acetonitrile (99.8%, Sigma-Aldrich). The films were fabricated by casting the solutions onto Teflon molds, followed by acetonitrile evaporation at 60 °C. Subsequently, the obtained films were dried at 110 °C for 36 h under vacuum. The resulting films with a thickness of ~200 μm were peeled off from the Teflon molds.

2.2. Differential Scanning Calorimetry. A DSC Q200 (TA Instruments) system was used for differential scanning calorimetry (DSC) measurements in the temperature range from −70 to 160 °C with a scan rate of 10 K min^{-1}. The heat flow was normalized by sample mass.

2.3. X-ray Diffraction. A STOE STADI MP-287 system was used for X-ray diffraction (XRD) measurements of polymer electrolytes at ambient temperature. Polymer electrolyte films with a diameter of 12 mm and a thickness of ca. 200 μm were sandwiched between two mylar foils. A copper source ($\lambda_{CuK\alpha1}$ = 1.54060 Å) was used for the measurements in the 2θ range from 2 to 70° with 2θ = 0.015° steps. XRD pattern of the $K_2Fe[Fe(CN)_6]$ cathode material was collected on an X-ray powder diffractometer Huber G670 with transmission geometry equipped with a linear PSD detector ($\lambda_{CoK\alpha1}$ = 1.78892 Å) in the 2θ range from 4 to 100° with 2θ = 0.005° steps.

2.4. Oscillatory Rheology. Small amplitude oscillatory shear (SAOS) tests were performed on a strain-controlled ARES G2 (TA Instruments) rheometer using 8 mm parallel plate geometry. All tests were conducted from 0.1 to 100 rad s^{-1} at low shear strains from 0.1 to 1% in the temperature range from 25 to 65 °C in 10 °C steps under nitrogen. Polymer electrolyte films with a diameter of 8 mm and a thickness of 0.5 mm were used for the measurements.

2.5. Ionic Conductivity Measurements. Polymer electrolyte films were cut off with a diameter of 8 mm and sandwiched between two stainless steel electrodes in a Swagelok-type setup. Prior to the measurement, the Swagelok-type cells were preconditioned in a temperature chamber at 60 °C for 12 h to improve the interfacial contact between the polymer films and electrodes. Electrochemical impedance spectroscopy (EIS) measurements were conducted on a Biologic SP-200 potentiostat at the frequency range from 1 MHz to 500 mHz (and reverse) with an amplitude of 20 mV in the temperature range from 5 to 85 °C in 10 °C steps. The temperature increasing rate was 1 °C min^{-1} over 10 min, and each temperature was held constant for 50 min to record impedance spectra. At 85 °C, the heating profile was reversed and cooled down to 5 °C under similar conditions. The bulk resistance (R_b) was further estimated from the Nyquist plot (exemplary given in Figure S1), and the ionic conductivity (σ) was calculated according to the following equation: $\sigma = (1/R_b)\cdot(l/A)$, where l is the film thickness and A is the film area.

2.6. Synthesis of $K_2Fe[Fe(CN)_6]$. PBA $K_2Fe[Fe(CN)_6]$ was synthesized via a co-precipitation method reported elsewhere.[4,26,27] Three solutions were prepared: (a) 0.782 g of $FeSO_4\cdot7H_2O$ (99%, Ruskhim) and 0.100 g of polyvinylpyrrolidone (M_w = 40.000, Sigma-Aldrich) in 20 mL of deionized water, (b) 0.244 g of $Na_3Cit\cdot5.5H_2O$ (99.5%, Ruskhim) in 10 mL of deionized water, and (c) 1.268 g of $K_4Fe(CN)_6\cdot3H_2O$ (99%, Ruskhim) in 10 mL of deionized water. The solutions were added to the vessel in the order (a), (b), and (c). The resulting suspension was stirred for 36 h at ambient temperature. Subsequently, the resulting precipitate was centrifuged and washed with a mixture of ethanol and deionized water (1:1 ratio by volume) several times and dried at 110 °C for 12 h under vacuum (10^{-3} mbar). After drying, the obtained powder was ground using a mortar.

2.7. Positive Electrode Preparation. For the preparation of positive electrodes for electrochemical tests with the LE, 0.180 g of the as-synthesized $K_2Fe[Fe(CN)_6]$, 0.090 g of carbon black ("CB", SuperP, Imerys Graphite & Carbon), and 0.030 g of PVdF (HSV900, GelonLib) (60:30:10 ratio by mass) were weighed in a ball-mill container, and 3 mL of *N*-methyl-2-pyrrolidone (99.5%, Sigma-Aldrich) was added. The container was transferred to a ball-mill mixer SPEX 8000, and the slurry was mixed for 1 h. Subsequently, the slurry was spread onto a conductive carbon-coated aluminum foil using an automatic film applicator Zehntner ZAA 2300 with a gap width of 150 μm and dried after deposition at 60 °C. In order to make the thickness and surface uniform, the electrode sheet was roll-pressed to a thickness of ~40 μm with a mass loading of ~1 mg cm^{-2}. Round-shaped electrodes with a diameter of 16 mm were cut out and dried at 110 °C for 12 h under vacuum (10^{-3} mbar) prior to use. Positive electrodes for electrochemical tests with SPEs were prepared according to the same sequence of procedures as described above.

For solid electrolyte cell configurations, the cathode composition was altered to accommodate a fraction of solid electrolyte in the electrode composite. In addition to the above components ($K_2Fe[Fe(CN)_6]$, CB, PVdF; w/w/w = 60:30:10), 0.030 g of PEO (average M_v = 100,000, Sigma-Aldrich, lot # MKCC5482) and 0.010 g of KTFSI (99.5%, Solvionic) were added to the slurry, corresponding to a EO:K ratio of 20:1 and an overall electrode composition of $K_2Fe[Fe(CN)_6]$:CB:PVdF:PEO:KTFSI = 52.9:26.5:8.8:8.8:2.9. In addition, the PEO:KTFSI 20:1 electrolyte was also tested with a slightly higher KTFSI content of 0.014 g (corresponding to a EO:K ratio of 16:1) concentration in the cathode blend (denoted "cell 2"), resulting in an overall composition of $K_2Fe[Fe(CN)_6]$:CB:PVdF:PEO:KTFSI = 52.3:26.2:8.7:8.7:4.1.

2.8. Electrochemical Characterization. Liquid and solid potassium batteries were studied in galvanostatic cycling experiments and rate capability tests.

2.8.1. Galvanostatic Cycling. The stainless steel CR2032 coin-type cells were assembled for the galvanostatic cycling tests, employing a

https://doi.org/10.1021/acsapm.2c00014
ACS Appl. Polym. Mater. XXXX, XXX, XXX−XXX

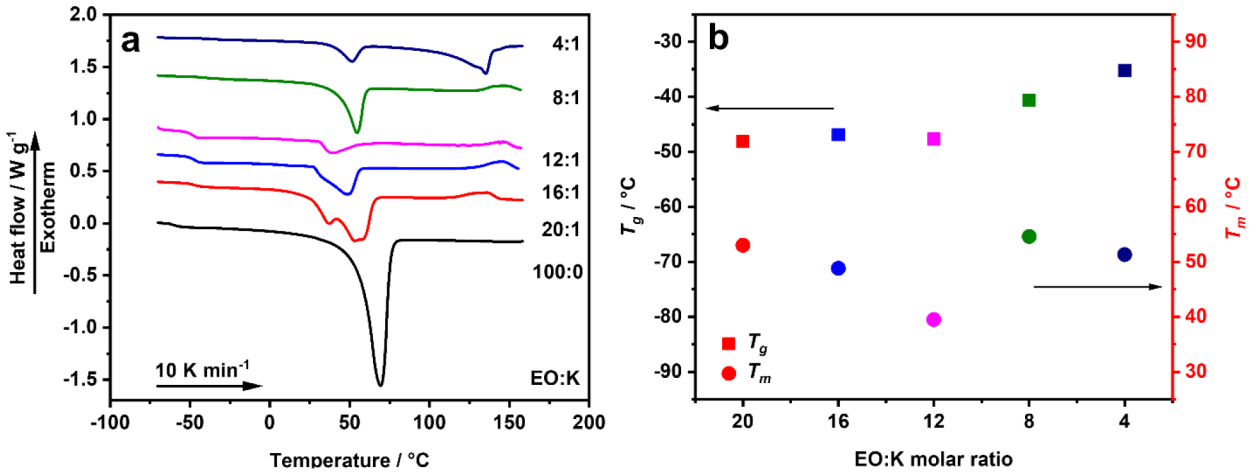

Figure 1. (a) DSC scans (heating scan rate of 10 K min^{-1}) of PEO-KTFSI blends employing different EO:K molar ratios and pure PEO (EO:K = 100:0). (b) Dependence of T_g and T_m values on the EO:K molar ratio in PEO-KTFSI blends.

Table 1. Summarized Data on Thermal Properties (T_g, T_m, ΔH_m, and Crystallinity) and Ionic Conductivity (σ) at 25 and 55 °C of PEO-KTFSI-Based Polymer Electrolytes Employing Different EO:K Molar Ratios

entry	EO:K ratio	T_g, °C	T_m, °C	ΔH_m, J/g	crystallinity[a], %	σ (25 °C), S/cm	σ (55 °C), S/cm
1	100:0	−59.8	69.2	126.2[b]	64.3[b]		
2	20:1	−48.1	53.0/37.0	68.1	34.7	1.30×10^{-6}	2.86×10^{-4}
3	16:1	−46.9	48.8	27.5	14.0	3.56×10^{-5}	6.77×10^{-4}
4	12:1	−47.7	39.5	11.1	5.7	1.91×10^{-5}	1.84×10^{-4}
5	8:1	−40.6	54.6	30.2	15.4	1.79×10^{-7}	6.18×10^{-5}
6	4:1	−35.2	51.3/135.2	38.5	19.6	4.01×10^{-8}	3.03×10^{-5}

[a]ΔH_m (PEO) theoretical = 196.4 J/g.[39] [b]Predried molten and thus not completely recrystallized PEO was used, and its crystallinity was calculated relatively to the theoretical ΔH_m of PEO as well as for all PEO-KTFSI blends.

$K_2Fe[Fe(CN)_6]$ positive electrode and a K-metal (98% stored in mineral oil, Sigma-Aldrich) negative electrode. For the reference cells with the LE, glass fiber separators (Whatman GF/B) were dried at 110 °C for 12 h under vacuum (10^{-3} mbar), and one layer of the separator was soaked with 150 μL of an electrolyte comprising a 0.5 M KPF_6 (99%, AcrosOrganics) solution in a mixture of ethylene carbonate (EC) (99%, Sigma-Aldrich) and propylene carbonate (PC) (99.7%, Sigma-Aldrich) (1:1 ratio by volume) with 2 wt % of fluoroethylene carbonate (FEC) (≥99%, Sigma-Aldrich). For the cells with SPEs, the polymer films with a diameter of 16 mm and a thickness of ∼200 μm were cut out and used as both electrolytes and separators. The galvanostatic cycling tests were conducted on a Neware BTS4000 battery test system. The SPE-based cells were preconditioned in a temperature chamber at 55 °C for 20 h prior to the following cycling at this temperature. The LE-based cells were preconditioned at ambient temperature (20 °C) for 2 h prior to the following cycling at this temperature. In both cases, the cycling rate was C/25 (1C = 155 mAh/g with respect to the theoretical capacity of $K_2Fe[Fe(CN)_6]$), and the voltage cut-offs were 2.5 and 4.3 V vs K^+/K.

2.8.2. Rate Capability Tests. The rate capability test was conducted on a Biologic BSC potentiostat. The cell composed of a $K_2Fe[Fe(CN)_6]$ positive electrode, a K-metal negative electrode, and a PEO-KTFSI EO:K = 20:1 SPE film with a diameter of 16 mm and a thickness of ∼200 μm was preconditioned in a temperature chamber at 55 °C for 20 h prior to the following cycling at this temperature. The cell was cycled using a constant current−constant voltage (CC−CV) cycling protocol.[28] CC-steps were performed at cycling rates of C/25, C/15, C/10, and C/5 increasing every five cycles. The sequences of three CC−CV cycles at C/25 were introduced between different cycling rates. The cutoff current in the CV-step was equivalent to the current at a rate of C/25, and the voltage cut-offs were 2.5 and 4.3 V vs K^+/K.

3. RESULTS AND DISCUSSION

3.1. Thermal Properties and Morphology of PEO-KFTSI Electrolytes. Primarily, the thermal properties of the series of PEO_x-$KTFSI_y$ blends with the ratio of x:y corresponding to different EO:K molar ratios (20:1, 16:1, 12:1, 8:1, 4:1) and pristine pure PEO were characterized by DSC (Figure 1a, summary given in Table 1). It is well known that the segmental motion of the amorphous PEO chains is a major pathway in the ion transport mechanism in PEO-based blends.[29] Therefore, lower T_g values as well as a lower crystalline fraction of PEO generally indicate enhanced ionic conductivity in these systems.[30,31] To identify the T_g value and melting transitions in a single experiment, a heating rate of 10 K min^{-1} was chosen, which is a common heating rate for polymer electrolytes.[32,33] Moreover, the heating rate was found to be a compromise since higher heating rates would facilitate identification of T_g values, while lower heating rates would result in more pronounced melting transitions.[34]

The pristine PEO featured a T_g at −59.8 °C, whereas PEO-KTFSI blends showed a predominant tendency of T_g shift toward higher temperatures with increasing salt content (Figure 1b). This trend can be explained by quasi-ionic cross-linking[35−37] as the result of the K^+-ion coordination by different segments of the polymer chains, leading to their physical cross-links, and thereby partial immobilization and restricted segmental motion.[19] Simultaneously, the melting point T_m decreased from 69.2 °C for pure PEO to melting points below 55 °C for PEO-KTFSI blends. As can be clearly seen in Figure 1b, polymer mixtures featured decreasing T_m values as the EO:K ratio changed from 20:1 to 12:1, which is

https://doi.org/10.1021/acsapm.2c00014
ACS Appl. Polym. Mater. XXXX, XXX, XXX−XXX

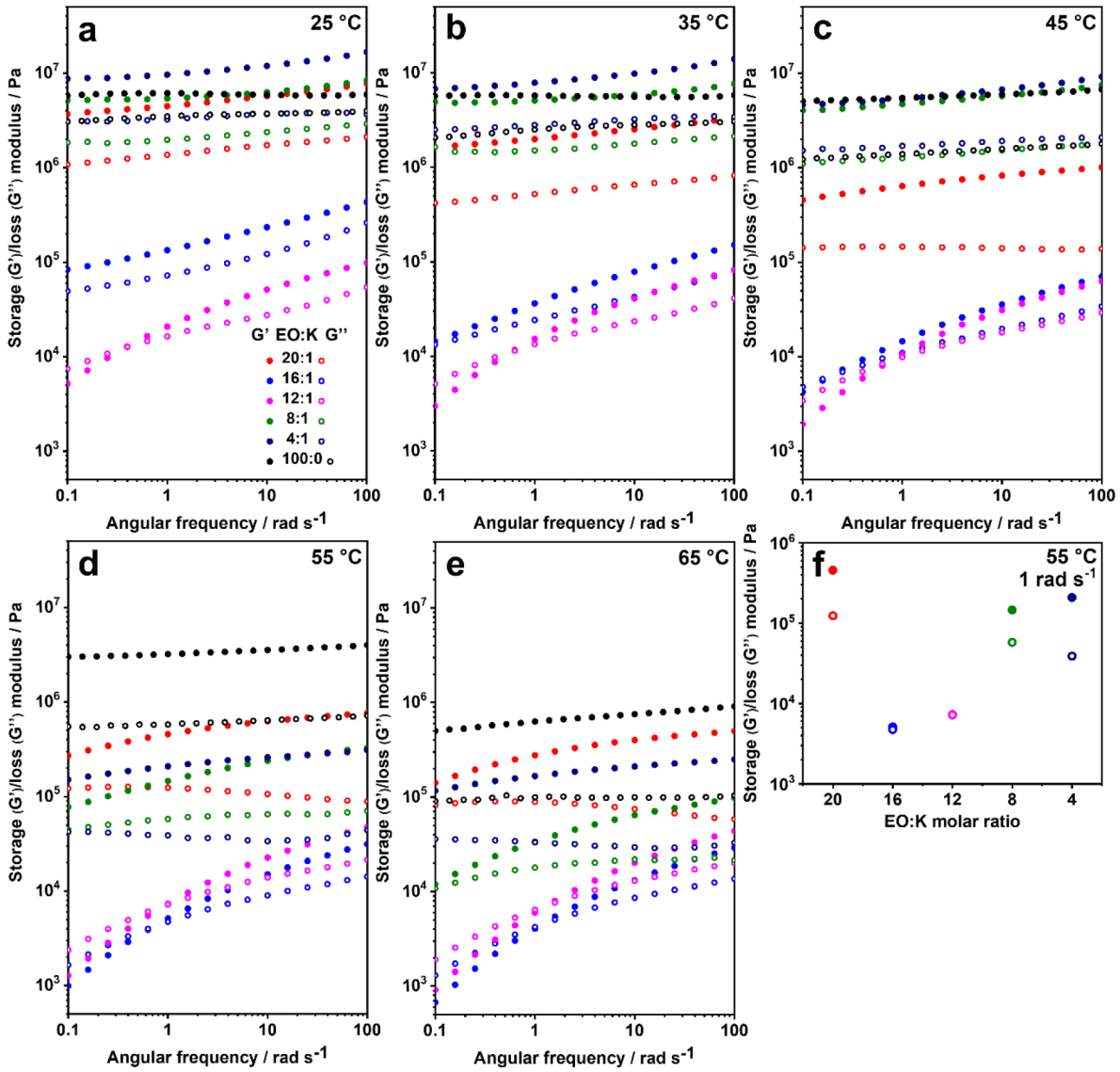

Figure 2. Dependence of storage (G′, full circles) and loss (G″, empty circles) moduli of PEO-KTFSI blends employing different EO:K molar ratios on angular frequency at (a) 25 °C, (b) 35 °C, (c) 45 °C, (d) 55 °C, and (e) 65 °C. (f) Dependence of storage and loss moduli on the EO:K molar ratio of PEO-KTFSI blends at an angular frequency of 1 rad s^{-1} at 55 °C.

likely a result of the plasticizing effect of the bulky $TFSI^-$ anions.[38] This is reflected in the declining trend of melting enthalpies (ΔH_m) from pure PEO (196.4 J/g)[39] to the 12:1 blend (11.1 J/g, given in Table 1) corresponding to the substantial reduction of the degree of crystallinity. As the KTFSI content further increased (EO:K = 8:1), both T_m and ΔH_m increased again, which is likely related to the formation of crystalline intermediate compounds.[40] Surpassing the saturation limit of EO:K = 5,[24,40] the concentration regime changed from salt-in-polymer to polymer-in-salt.[41,42] Thus, in the DSC scan of PEO_4-$KTFSI_1$, an additional endothermic peak at 135 °C was clearly observed, corresponding to the phase reported in the literature as the molar ratio of EO:K = 1.5:1.[24] A mixed-phase system was also observed in the case of PEO_{20}-$KTFSI_1$ that manifests an additional phase with a lower melting point (T_m = 37 °C). Contrary to the PEO-LiTFSI blends,[24,40] a crystallinity gap for the investigated EO:K molar ratios was not detected. Moreover, a rearrangement process for PEO-KTFSI blends occurred at high temperatures (above 115 °C), which is confirmed by the appearance of exothermic peaks.

To investigate the morphology of the PEO-KTFSI blends, XRD measurements were conducted for the compositions with a different salt content at ambient temperature (Figure S2). For the pure PEO, a single reflection at 2θ = 19° and three overlapping reflections at around 23° were observed, corresponding to a monoclinic structure[43] and being in agreement with the values reported in the literature.[44,45] For PEO_{20}-$KTFSI_1$, the appearance of additional reflections was manifested, which are the most intense around 2θ = 11, 14, and 20° and likely correspond to the phase with a molar ratio of EO:K = 20:1, while the characteristic PEO reflections still remained. For PEO_{16}-$KTFSI_1$ and PEO_{12}-$KTFSI_1$ blends, much broader reflections were observed, which are attributed to the presence of an amorphous phase in their XRD patterns.[46] This correlates well with the thermal properties of these compositions, in particular with their lower crystallinity in comparison to other PEO-KTFSI blends (Table 1). As the molar ratio of EO:K approached 8:1, the characteristic PEO

https://doi.org/10.1021/acsapm.2c00014
ACS Appl. Polym. Mater. XXXX, XXX, XXX−XXX

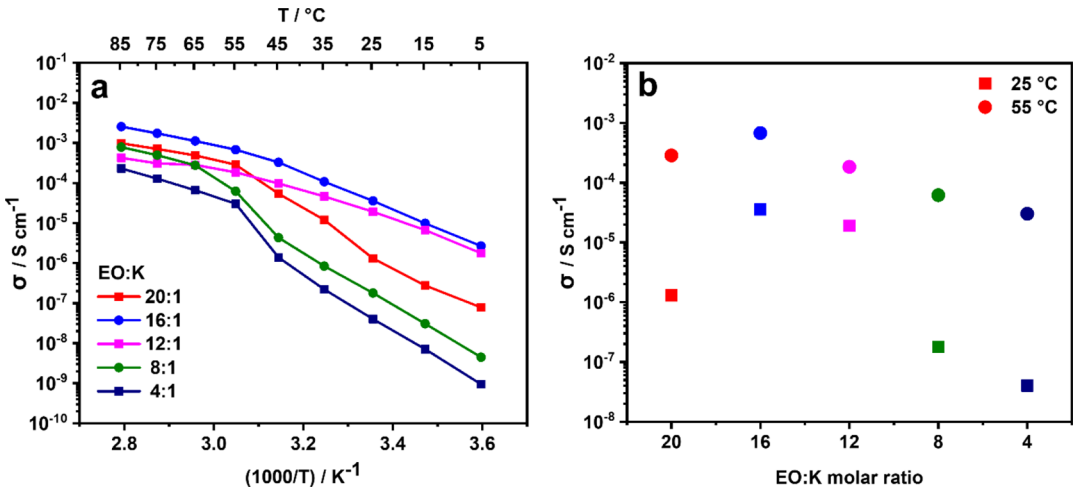

Figure 3. (a) Temperature-dependent ionic conductivity of PEO-KTFSI blends employing different EO:K molar ratios derived from the EIS measurements in the temperature range from 5 to 85 °C. (b) Dependence of ionic conductivity on the EO:K molar ratio in PEO-KTFSI blends at 25 and 55 °C.

reflections disappeared, while the number of additional reflections grew. In the XRD patterns of PEO_8-$KTFSI_1$ and PEO_4-$KTFSI_1$, these reflections are likely attributed not only to the eutectic phases with molar ratios of EO:K = 8:1 and 4:1 but also to the crystalline intermediate compounds. Furthermore, no sign of characteristic KTFSI reflections (shown in Figure S2, EO:K = 0:100) in the XRD patterns of the investigated PEO-KTFSI blends indicates the absence of the "free" crystalline salt in these compositions. In general, the findings of the XRD analysis reflect the DSC results discussed above: the mostly amorphous state of PEO_{16}-$KTFSI_1$ and PEO_{12}-$KTFSI_1$ compared to that of other blends and the appearance of ion−ion interactions in compositions with a higher salt content.

To summarize, the KTFSI content in the polymer blends should be chosen carefully since $TFSI^-$ anions strongly contribute to crystallinity suppression, while at the same time, cations participate in ion−ion interactions and quasi-ionic cross-linking, thus reducing the PEO chain mobility.

3.2. Rheological Properties of PEO-KTFSI Polymer Electrolytes. SAOS test was used to evaluate the influence of KTFSI concentration on the rheological properties of the PEO-based electrolyte films. The storage (G′) and loss (G″) moduli of PEO-KTFSI blends were measured from 0.1 to 100 rad s^{-1} at low shear strains from 0.1 to 1% in the temperature range from 25 to 65 °C in 10 °C steps (Figure 2a−e) to be within the linear regime. In viscoelastic materials, G′ is ascribed to the elastic portion or solid-state behavior and G″ can be seen as the viscous portion or liquid-like behavior of the polymer sample.[47,48] Under the influence of shear and/or temperature, the value of G″ can exceed the magnitude of G′ and the sample starts to flow, thus losing its structural integrity. However, maintaining the structural integrity is highly relevant for the SPE as it acts both as an electrolyte and a separating layer between the anode and cathode, thus suppressing dendrite formation and preventing short-circuits.[33] In general, SPEs can gain the mechanical strength from a rigid crystalline phase of the polymer or cross-links due to ion−polymer interactions,[49] restricting the polymer chain motion and contributing to a structural integrity. Herein, the predominant contribution of these effects to the mechanical properties of PEO-based compositions depending on their KTFSI content is discussed. As demonstrated in Figure 2, for the PEO_4-$KTFSI_1$, PEO_8-$KTFSI_1$, and PEO_{20}-$KTFSI_1$ blends as well as for pure PEO, the storage modulus dominated over the whole temperature range investigated (G′ > G″), thus providing the desired solid-state behavior. However, the mechanical strength of these materials was likely provided by different effects: pristine PEO and PEO_{20}-$KTFSI_1$ possessed the highest crystallinity degrees (Table 1), while PEO_8-$KTFSI_1$ and PEO_4-$KTFSI_1$ exhibited the highest T_g values due to a large number of quasi-ionic cross-links. At temperatures below T_m (Figure 2a−c), PEO_4-$KTFSI_1$ and PEO_8-$KTFSI_1$ demonstrated the highest storage and loss moduli among all blends. It is noteworthy that in the temperature range of 25−35 °C, the storage modulus of the PEO_4-$KTFSI_1$ blend was higher as compared to that in the pristine polymer, indicating the significant contribution of cross-links to the improvement of structural integrity. Moreover, both PEO_4-$KTFSI_1$ and PEO_8-$KTFSI_1$ maintained the mechanical strength below T_m, and only a negligible decline of their moduli along with the temperature increase was observed. In contrast, PEO_{20}-$KTFSI_1$, the blend with the lowest T_g but the highest crystallinity, exhibited a significant decrease of its moduli in the same temperature range (Figure 2a−c). This correlates with PEO_{20}-$KTFSI_1$ thermal properties, reflecting the loss of structural integrity of an additional crystalline phase with a lower melting point (T_m = 37 °C, Figure 1a and Table 1). Surpassing T_m of PEO_4-$KTFSI_1$ and PEO_8-$KTFSI_1$, the rigid crystalline phase melted and consequently lost its mechanical integrity, which was dramatically reflected in changed rheological properties (Figure 2d). In contrast, PEO_{20}-$KTFSI_1$ possessed the highest moduli compared to other blends at temperatures above T_m (Figure 2d,e). This might be attributed to the fact that PEO_{20}-$KTFSI_1$ employed a lower amount of bulky $TFSI^-$ anions in comparison to other blends, thus possessing less hindered polymer chain alignment. Therefore, the rheological properties of this blend are expected to be the closest to that of pristine PEO, which displayed the highest values of G′ and G″ above 55 °C. In Figure 2e, the significant moduli decline can be seen for the pure polymer, when approaching its T_m (69.2 °C, Table 1), however, still possessing the highest moduli in comparison to all blends.

https://doi.org/10.1021/acsapm.2c00014
ACS Appl. Polym. Mater. XXXX, XXX, XXX−XXX

As discussed above, PEO_{12}-$KTFSI_1$ and PEO_{16}-$KTFSI_1$ exhibited the lowest T_m and crystallinity degrees (Table 1). In accordance with their thermal properties, the lowest values of both G′ and G″ were found over the investigated temperature range. Moreover, for PEO_{12}-$KTFSI_1$, the trend G″ > G′ was observed in the low-frequency region, indicating the dominance of liquid material properties. As the frequency increased, the trend G″ = G′ (crossover or yield point) was observed, followed by G′ > G″ at high values of frequency. The crossover point shifted as expected toward higher frequency values with increasing temperature, showing that the frequency domain in which liquid-like behavior is observed expands as a function of temperature. This can be explained by the simultaneous increase of polymer chain motion in PEO_{12}-$KTFSI_1$. It is noteworthy that similar tendency was manifested for PEO_{16}-$KTFSI_1$ above its T_m. For application in a battery cell, this behavior is not suitable as the polymer electrolyte films also act as a separator between the electrodes. Therefore, liquid-like behavior would lead to a depletion of the polymer between the electrodes under the constant stack pressure in the cell and thus to rapid short-circuits and cell failure.

To summarize, the mechanical properties were found to depend on three competing effects, each dominating at different KTFSI concentration regimes: (1) the degree of crystallinity (PEO_{20}-$KTFSI_1$), (2) the plasticizing effect of $TFSI^-$ anions (PEO_{12}-$KTFSI_1$ and PEO_{16}-$KTFSI_1$), and (3) quasi-ionic cross-linking effect (PEO_8-$KTFSI_1$ and PEO_4-$KTFSI_1$). The influence of each predominant effect on the mechanical strength of the blends can be clearly seen in Figure 2f, where the dependence of the storage and loss moduli on the EO:K molar ratio at an angular frequency of 1 rad s^{-1} and a temperature of 55 °C is shown. The amorphous nature of PEO_{12}-$KTFSI_1$ and PEO_{16}-$KTFSI_1$, the result of the $TFSI^-$ anion plasticizing effect, adversely affected their mechanical strength, while blends with a higher number of cross-links and/or a higher degree of crystallinity yielded electrolyte films with higher moduli and hence better mechanical stability.

3.3. Ionic Conductivity Experiments. Temperature-dependent EIS measurements were conducted for the PEO-KTFSI blends with different EO:K molar ratios to determine their ionic conductivity in the temperature range from 5 to 85 °C (Figure 3a). The conductivity performances of PEO-KTFSI blends at 25 and 55 °C (below and above their T_m, respectively) are presented in Figure 3b for further discussion of the influence of the KTFSI content on the ionic conductivity.

At first, the increase of ionic conductivity can be seen as the EO:K molar ratio changed from 20:1 to 16:1 due to simultaneous crystallinity decline and increase of the number of charge carriers. PEO_{16}-$KTFSI_1$ demonstrated the highest values of ionic conductivity over the investigated temperature range as compared to other PEO-KTFSI blends. As given in Table 1, PEO_{16}-$KTFSI_1$ possessed 3.56×10^{-5} S/cm at 25 °C. For comparison, a literature reference of the PEO-LiTFSI system with a molar ratio of EO:Li = 15:1 featured comparatively a similar ionic conductivity of 3.54×10^{-5} S/cm at ambient temperature.[50] Nevertheless, a precise comparison of the conductivity characteristics of PEO-KTFSI and PEO-LiTFSI is difficult since the reported values of the PEO-LiTFSI conductivity vary widely.[50−52] Although the ionic conductivities of PEO-Li/KTFSI systems are similar, higher cation mobility can be expected for the system based on K^+ owing to its larger size, resulting in a lower dissociation energy of the salt,[23,24] which potentially enables enhanced ion transport properties. Literature values for a comparable PEO-based electrolyte employing the FSI-salt instead of TFSI were recently provided by Fei et al.[20] Therein, it was reported that PEO_{10}-KFSI possessed the highest ionic conductivity of 1.14×10^{-5} S/cm at 40 °C. It is noteworthy that compared to reported results, the PEO_{16}-$KTFSI_1$ blend investigated herein demonstrated ionic conductivity in the same order of magnitude at a lower temperature of 25 °C. In fact, its ionic conductivity is 1 order of magnitude higher at 40 °C (2.08×10^{-4} S/cm, estimated from Figure 3a). The (PPC)-KFSI-modified cellulose membrane proposed as the SPE for the K-based cell in another study by Fei et al.[10] demonstrated an ionic conductivity of 1.36×10^{-5} S/cm at 20 °C, which is comparably close to that of PEO_{16}-$KTFSI_1$ at 25 °C.

Furthermore, it can be seen in Figure 3b that the described trends were less visible at temperatures above the melting point of PEO-KTFSI blends, presumably due to the absence of crystalline regions. In contrast to other compositions, PEO_{16}-$KTFSI_1$ and PEO_{12}-$KTFSI_1$ possessed already a low degree of crystallinity and consequently did not exhibit an equally dramatic change in ionic conductivity over up to 3 orders of magnitude at elevated temperatures (Figure 3b).

3.4. Discussion: Physical Properties of PEO-KTFSI Polymer Electrolytes. Following the general hypothesis that a higher fraction of the amorphous phase results in higher ionic conductivities, the conductivity value would be expected to increase from PEO_{20}-$KTFSI_1$ to PEO_{12}-$KTFSI_1$ (Figure 1, Table 1). This is generally motivated by larger degrees of segmental and transitional (i.e., ion hopping mechanism) motion that promotes inter- and intramolecular ion movement.[53−55] Although the PEO_{12}-$KTFSI_1$ blend showed the lowest T_m and the lowest degree of crystallinity (XRD results, Figure S2), in practice, the highest ionic conductivity was found for the PEO_{16}-$KTFSI_1$ blend. In fact, increasing the KTFSI salt content from the 16:1 to 4:1 ratio, yielded a continuous decrease of the ionic conductivity (Figure 3b). This is because counteracting structural effects such as quasi-ionic cross-links and potassium coordination have to be taken into account as well. For instance, as the concentration of potassium ions increases, an increasing number of oxygen atoms in the PEO chain will be coordinated to potassium ions. This alters both dynamic segmental motion and the availability of coordination sites. It is known that the coordination number for Li^+ in PEO is 6.[56,57] To our knowledge, for the PEO-KTFSI system, coordination geometry has not been investigated in detail yet. However, it is reasonable to assume that larger cations lead to higher coordination numbers. However, different coordination geometries and binding strength can have a strong impact. For our series of PEO-KTFSI, this specifically means that lower ionic conductivities are presumably related to a large degree of occupied hopping sites,the presence of crystalline intermediate compounds (i.e. additional phases with different ionic conductivity), and a higher number of quasi-ionic cross-links.[35,36,19] This is also indicated in major changes in the XRD pattern between PEO_8-$KTFSI_1$ and PEO_4-$KTFSI_1$.

In conclusion, it can be assumed that PEO_{16}-$KTFSI_1$ and PEO_{12}-$KTFSI_1$ are the most promising candidates for the application as SPEs in potassium batteries owing to their comparatively high ionic conductivities, especially below their melting points. However, as shown in the discussion of rheological properties, their amorphous nature adversely

https://doi.org/10.1021/acsapm.2c00014
ACS Appl. Polym. Mater. XXXX, XXX, XXX−XXX

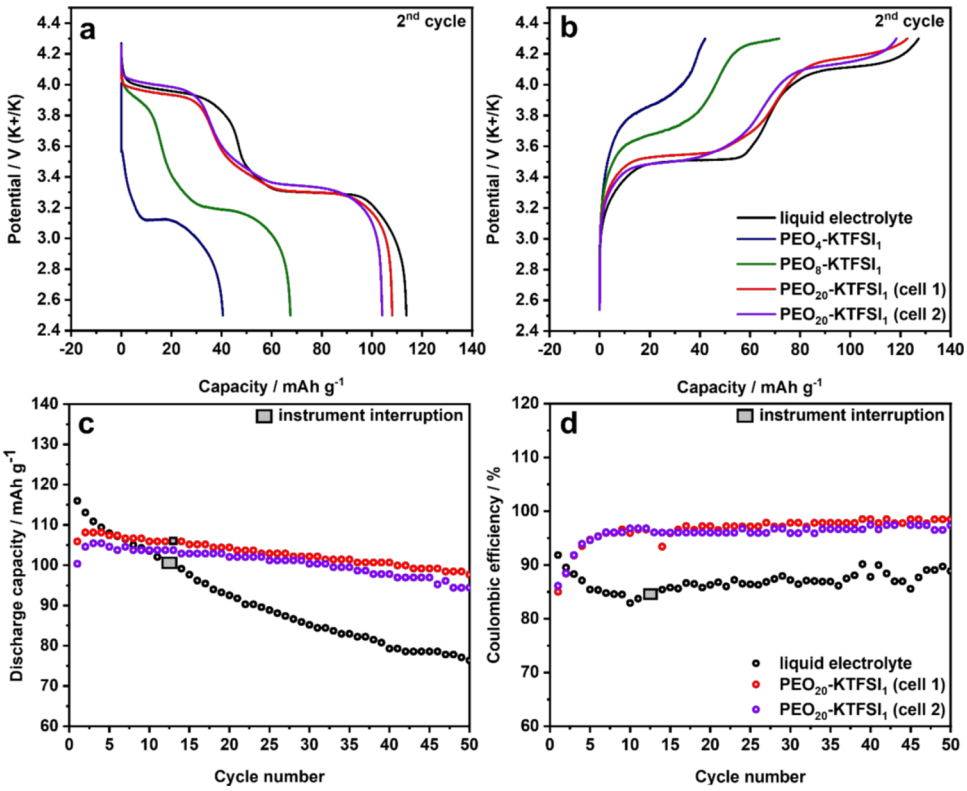

Figure 4. Comparison of potassium half-cells employing different electrolyte systems. (a) Galvanostatic discharge profiles in the second cycle. (b) Galvanostatic charge profiles in the second cycle. (c) Capacity retention and (d) corresponding CEs.

affected the mechanical stability, and therefore, free-standing films could not be obtained, which is a prerequisite for the practical application in solid-state PIBs. In contrast, the blends having a higher degree of crystallinity yielded processable free-standing films that were capable of keeping the anode and cathode separated. Based on the data presented above, we chose PEO_4-$KTFSI_1$, PEO_8-$KTFSI_1$, and PEO_{20}-$KTFSI_1$ blends for electrochemical testing in the following chapter as these three compositions provided sufficient mechanical strength despite the modest ionic conductivities at elevated temperatures. Among these three polymer electrolytes, the PEO_{20}-$KTFSI_1$ composition possessed the best trade-off between the ion transport and mechanical properties.

3.5. Electrochemical Measurements. For cell tests in K-metal/electrolyte/cathode configurations, PBA $K_2Fe[Fe(CN)_6]$ was synthesized by the precipitation method.[4] The material was chosen for its remarkable cycling stability, as shown in previous studies.[4,58] In addition, the material purely iron-based and free of critical heavy metals such as cobalt or nickel rendered this material more sustainable. Powder diffraction performed on the obtained material showed an XRD pattern (Figure S3) characteristic to the monoclinic structure (S.G. *Pc*) of $K_2Fe[Fe(CN)_6]$ from which the unit cell parameters were determined as follows: a = 6.8777(8) Å, b = 14.792(2) Å, c = 12.133(1) Å, β = 123.420(7)°.[8] The significant broadening of the diffraction peaks can be likely attributed to a small particle size.

3.5.1. Capacity Retention in Galvanostatic Cycling Experiments. The electrochemical performance of PEO-KTFSI SPEs with molar ratios of EO:K = 4:1, 8:1, 20:1 was compared to that of a LE, the reference system, comprising a solution of KPF_6 in ethylene carbonate (EC) and propylene carbonate (PC) with 2 wt % of the fluoroethylene carbonate (FEC) additive (see the Experimental Section) to suppress electrode−electrolyte side reactions. The EC:PC solvent mixture has been reported as a particularly stable combination toward oxidation in the high-voltage region.[11] Furthermore, KTFSI was avoided as the electrolyte salt as it may induce corrosion processes at the Al current collector.[4] Because of the comparatively low ionic conductivity at room temperature, galvanostatic cycling of SPE-based cells was carried out at 55 °C, while the reference LE-based cell was tested at ambient temperature (20 °C) (Figure S4). In both cases, the cycling rate was C/25 with a voltage window of 2.5−4.3 V vs K^+/K. In Figure S4a, only 7 cycles are shown for the cell employing PEO_4-$KTFSI_1$ due to its failure afterward, while the cell with PEO_8-$KTFSI_1$ SPE failed after 45 cycles (Figure S4b). Both experiments were not repeated due to the observed high polarization resulting in low capacities. Meanwhile, the additional experiment was conducted for the cell based on the PEO_{20}-$KTFSI_1$ SPE (cell 1 and cell 2, shown in Figure S4c,d, respectively). Unlike cell 1, a higher concentration of the KTFSI salt additive in slurry for positive electrode preparation was used for cell 2 (see the Experimental Section). In this way, the electrode part could be possibly improved in terms of ion transport, potentially resulting in higher achievable capacities. However, it will be shown and discussed below that cell 2 showed no advantages over cell 1 with a lower salt content in the cathode slurry.

In Figure 4a−d, the cycling results of SPEs are shown. The galvanostatic profiles of SPEs in the first cycle (Figure S5) correspond to the conditioning process and are not discussed herein, while the discharge and charge profiles in the second cycle are presented in Figure 4a,b. It is noteworthy that

https://doi.org/10.1021/acsapm.2c00014
ACS Appl. Polym. Mater. XXXX, XXX, XXX−XXX

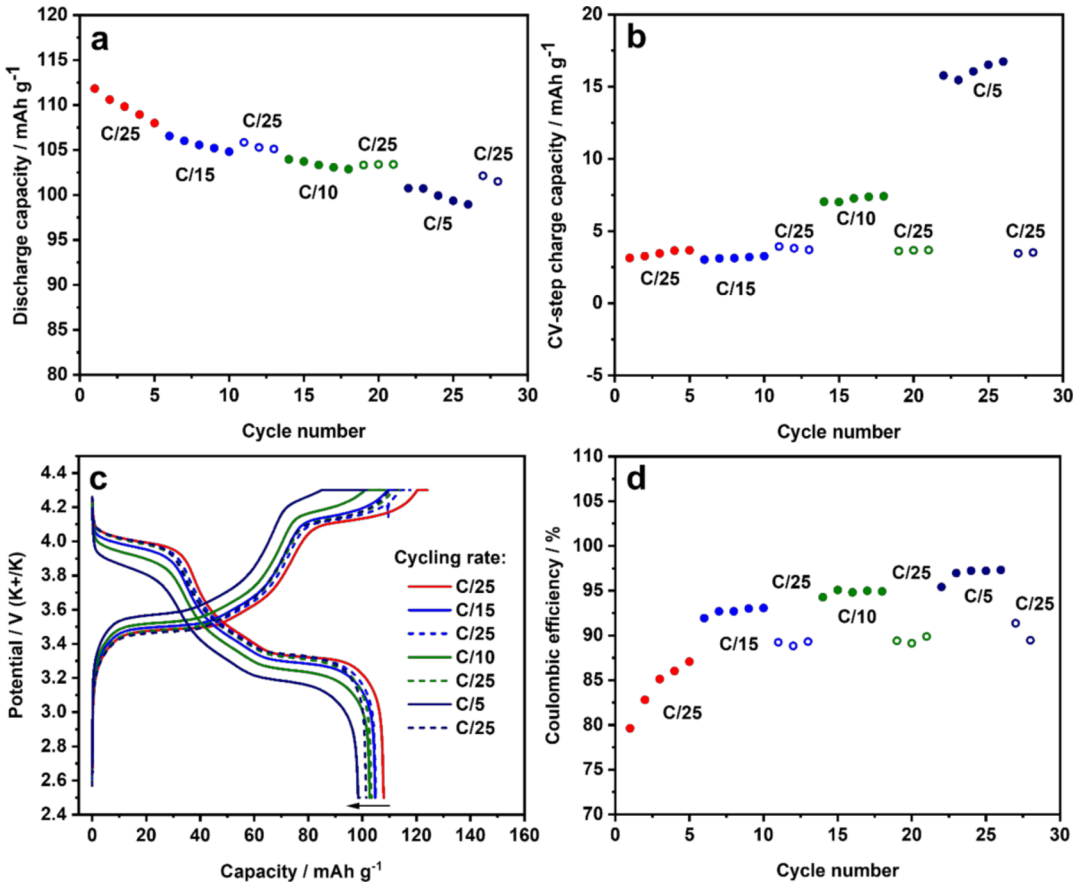

Figure 5. Rate capability test of the cell employing PEO_{20}-$KTFSI_1$ SPE. (a) Capacity retention. (b) Charge capacities reached in CV steps. (c) Galvanostatic charge and discharge profiles. (d) CEs at different cycling rates.

practical capacities of PBA-based electrodes depend on the chemical composition of electrode materials, whereas a lower amount of $[Fe(CN)_6]^{4-}$ vacancies results in an improved electrochemical performance.[26] For comparison, Bie et al. reported on a LE-based potassium half-cell composed of the PBA-based $K_{1.64}Fe[Fe(CN)_6]_{0.89}{\cdot}0.15H_2O$ cathode that delivered practical capacities of around 130 mAh g^{-1} (84% of the theoretical capacity calculated for the stoichiometry with the absence of $[Fe(CN)_6]^{4-}$ vacancies).[4] As can be seen in Figure 4a, a practical capacity of 108.1 mAh g^{-1} was delivered on the second cycle of the discharge process of cell 1 with the PEO_{20}-$KTFSI_1$ electrolyte, which is 70% of the theoretical capacity of $K_2Fe[Fe(CN)_6]$[4] and only 5% lower than that of the reference cell (113.1 mAh g^{-1}) with LE. Contrary to the assumption of the enhanced capacity in cell 2 employing a higher KTFSI concentration in the cathode slurry, it achieved a slightly lower discharge capacity of 104.6 mAh g^{-1}. This can be likely explained by a low mass loading of the active material (ca. 1 mg cm^{-2}) and thickness (ca. 40 μm) of the cathode, providing high accessibility of particles on its surface and thus resulting in a negligible effect of the additional conductive additive. One can assume that this effect is more pronounced in thicker electrodes, especially when operating at a high cycling rate, where an increased ion transport in the material is required due to the lack of surface contact between active material particles in deeper layers and SPE. Significantly lower discharge capacities were obtained in the second cycle of the cells employing PEO_8-$KTFSI_1$ and PEO_4-$KTFSI_1$ SPEs (67.2 and 40.5 mAh g^{-1}, respectively). In Figure 4a,b, two distinct voltage plateaus were observed for PEO_{20}-$KTFSI_1$ and LE, and only a negligible polarization effect was observed in the case of PEO_{20}-$KTFSI_1$ (changes in redox potentials $\Delta V < 0.06$ V), which indicates sufficient ionic conductivity at the chosen cycling rate and good interfacial compatibility with the cathode material. In contrast, the galvanostatic profiles of the cells employing PEO_8-$KTFSI_1$ and PEO_4-$KTFSI_1$ electrolytes exhibited significant polarization ($\Delta V \approx 0.2-0.4$ V) compared to the sample with LE. Therefore, the PEO_4-$KTFSI_1$ cell did not reach the second voltage plateau in the charge profile before the upper voltage cutoff (4.3 V) was reached. The PEO_8-$KTFSI_1$ cell showed the onset of the second plateau before the cycling was stopped at 4.3 V. This generally reflects well the differences of ionic conductivity depending on the KTFSI content (see Table 1).

As shown in Figure 4c, the benefit of using a solid electrolyte rather than a LE is the significantly improved capacity retention. Thus, the PEO_{20}-$KTFSI_1$ cells reached a capacity retention of 90% over the first 50 cycles, while the reference LE-based system retained only 66% of its initial capacity over the same cycle number interval (i.e., 36% improvement in capacity retention). In general, higher capacity retention indicates lower degrees of side reactions and therefore improved electrochemical stability of the SPE in comparison to that of the LE. This is further reflected in the CE, shown in Figure 4d, which will be discussed below. Higher electrochemical stability is strongly linked to the interface processes between the electrode and electrolyte. In a battery, the SEI acts as a protective layer suppressing excessive electrolyte

https://doi.org/10.1021/acsapm.2c00014
ACS Appl. Polym. Mater. XXXX, XXX, XXX−XXX

consumption. However, the nature and quality of the SEI may vary strongly in different electrolytes.[59] To further evaluate the SEI formed in the PEO_{20}-$KTFSI_1$ system, methods such as XPS and/or SEM can be suggested. However, the solid-state sample preparation is challenging as the cell components are fused after cycling, and therefore, the fragile SEI layer is readily damaged. More advanced approaches could be used in future studies, such as cryomicrotome to perform clean cross-sectional cuts through the cell stack.[60]

As can be seen in Figure 4c, the PEO_{20}-$KTFSI_1$ cells showed an increasing discharge capacity from the first to the following cycles. Cell 1 demonstrated the maximum discharge capacity in the second cycle (108.1 mAh g^{-1}, which is 2% higher compared to that in the first cycle), while cell 2 showed the highest discharge capacity in the third cycle (105.4 mAh g^{-1}, about 5% higher compared to that in the first cycle). This behavior was more pronounced in the PEO_4-$KTFSI_1$ cell (Figure S4a) that exhibited a considerably smaller initial discharge capacity, but the capacity continued to increase over the following cycles. In Figure S4b, a similar behavior was observed for the cell employing PEO_8-$KTFSI_1$. This behavior is generally attributed to the excluded electrode domains from the ion-conducting SPE due to the insufficient electrode−electrolyte surface contact and uncompleted penetration of SPE into the remaining cathode void space during the first cycles. Over time, polymer electrolytes creep further into the porous network of the cathode, which involves more active material particles.[20] It can be seen that the creeping process took longer for PEO_4-$KTFSI_1$ and PEO_8-$KTFSI_1$ SPEs, which can be attributed to their significant morphology change due to a gradual fade of crystalline intermediate ionic associates over time.

The analysis of CE is a measure of the degree of irreversible processes at the electrode−electrolyte interface during charge and discharge and is presented for PEO_{20}-$KTFSI_1$ and LE-based cells in Figure 4d. The CE data reveals a significant difference in both the SEI formation process on the first cycles and the long-term CE. In the first cycle, the cells based on PEO_{20}-$KTFSI_1$ demonstrated a CE of around 85%, which is 7% lower than that of the LE-based cell (92%). This can be addressed to a higher degree of irreversible reactions at the reactive potassium−SPE interface in the beginning of the experiment due to the elevated test temperature (55 °C instead of 20 °C for the LE). In the setup with a conventional LE, a significant drop of CE was observed on subsequent cycles (from 92% in the 1st cycle to 83% in the 10th cycle), indicating the gradual increase of side reactions typical for carbon-based electrolyte/K-metal setups,[4,61] leading to re-current electrolyte consumption and capacity fade. Meanwhile, the systems with the PEO_{20}-$KTFSI_1$ polymer electrolyte displayed CE increase and remained stable throughout subsequent cycles, approaching 98% in the 50th cycle.

3.5.2. Rate Capability of a K-Metal/PEO_{20}-$KTFSI_1$/$K_2Fe[Fe(CN)_6]$ Cell. In addition, a PEO_{20}-$KTFSI_1$ cell was built to study the rate capability of the system (Figure 5a−d). The experiment was conducted using the CC−CV technique (see the Experimental Section). The cycling rate was varied between C/25 and C/5 increasing every five cycles. Furthermore, a sequence of 3 CC−CV cycles at the slowest cycling rate (C/25) was introduced between increasing C-rates to ensure that the cell was not damaged at the higher current previously applied and also to reveal the practical capacity that can be still delivered by the cell.[28] The CV-step was introduced not only to improve the charge depth but also to reduce kinetic limitations at the end of charge/discharge that are known for charging Li-based batteries.[62−65] The discharge capacities obtained during the rate test are shown in Figure 5a. Compared to our previous CC long-cycling experiments (Figure 4c), the initial discharge capacity was slightly higher (112 mAh g^{-1}), which is a result of the CC−CV technique where the CV-step adds an additional contribution to the total charge capacity. Over the first 5 cycles at C/25, a continuous capacity fade was observed, contrary to the discussed above results of long-term cycling shown in Figure 4c. However, over the C/15 and C/10 rate steps, the capacity in the C/25 sequences leveled at 105.8 mAh g^{-1}, which is in agreement with the previously found discharge capacities after 20 cycles (Figure 4c). The fading rate slowed down when switching from C/25 to C/15 since generally the highest degree of side reactions is triggered during the first cycles. At the end of the C/15 sequence, a discharge capacity of 104.8 mAh g^{-1} was observed, which corresponds to the capacity retention of 94%. In the next higher rate step, for the C/10 sequence, a similar fading rate was observed to that in the C/15 step and a capacity of 102.8 mAh g^{-1} was delivered at the end of the fifth cycle (capacity retention of 92%). For the C/10 sequence, a slight increase in the capacity contribution transferred in the CV-step was observed (Figure 5b), while both C/15 and C/25 CV-sequences exhibited similar values. The maximum CV-step capacity was reached in the C/5 sequence (16.7 mAh g^{-1}), indicating that at this comparatively high rate, the charge ended prematurely. At the beginning of the C/5 sequence, a notable capacity drop compared to the previous C/25 sequence can be seen. However, a similar capacity fading trend over the five cycles as compared to previous C/15 and C/10 rate sequences was manifested. The following C/25 sequence further showed that about 91% of the initial capacity can be regained and thus being mainly a kinetic phenomenon. The associated capacity loss during each cycling sequence at a constant rate suggests that irreversible processes occurred, which impact the long-term capacity retention of the cell. This trend is also reflected in the polarization seen in the potential profiles in Figure 5c: a negligible polarization effect was observed while cycling at C/15 ($\Delta V \approx 0.04$ V compared to C/25), indicating a sufficient ion transport at this rate. The polarization was about twice as large during the cycling at C/10 ($\Delta V \approx 0.09$ V compared to C/25) and increased further at the next higher rate at C/5 ($\Delta V > 0.13$ V compared to C/25). More importantly, the onset of the second voltage plateau in the charge profile shifted notably, and the upper voltage cutoff of 4.3 V was reached earlier along with the rate increase. The constant voltage region at 4.3 V is a result of the CV-step and corresponds to the residual capacities contribution shown in Figure 5b.

Although discharge capacities were slightly smaller at higher rates and the cell tended to reside longer at the upper cutoff limit that could give rise to side reactions, it appears that with the CC−CV technique, higher rates deliver higher CEs. As can be seen in Figure 5d, for the C/25 intermediate sequences, a CE of ca. 90% was observed, while during the cycling at the highest rate of C/5, the CE reached values of around 97%. For comparison, the CE has been increasing over the first 10−15 cycles during our previous long-cycling experiments (Figure 4d), before the values approached a constant value of around 98%. Furthermore, the CE was generally lower than that shown in Figure 4d. This indicates that the capacity transferred

https://doi.org/10.1021/acsapm.2c00014
ACS Appl. Polym. Mater. XXXX, XXX, XXX−XXX

in the CV-step during charge is mostly ascribed to irreversible processes as the capacity apparently cannot be extracted reversibly on the following discharge. This highlights further that irreversible losses are associated with the time the cell resides at high potentials and is thus a function of the upper cutoff limit, CV-step time (and cutoff limitations), as well as the cycling rate in the CC-step. Hence, one can infer from these findings that faster rates result in the reduced degree of irreversible side reactions and thus improve the CE of the system.

3.5.3. Performance Comparisons with Reported SPE-Based Cells. Among recently introduced studies of solid-state potassium cells, Fei et al.[20] presented a potassium half-cell composed of a Ni_3S_2@Ni negative electrode and PEO-KFSI SPE operating at a current density of 25 mA g^{-1} at 55 °C, which delivered a practical discharge capacity of 312 mAh g^{-1} (18% lower than that achieved by the corresponding LE-based setup) and demonstrated a superior capacity retention of 98% over 100 cycles. However, the Ni_3S_2@Ni negative electrode was not tested against a positive electrode, which is a challenge in itself. Meanwhile, a solid-state potassium battery with an organic positive electrode, a potassium metal negative electrode, and a PPC-KFSI-modified cellulose membrane as the SPE operating at ambient temperature was introduced in another study of Fei et al.[10] The cell displayed a discharge capacity of 118 mAh g^{-1} at a current density of 10 mA g^{-1}, which was about 13% higher than that of the reference system with the LE. Moreover, a lower capacity fade was observed for the cell with the SPE, resulting in 84% capacity retention over 40 cycles, while the LE-based cell demonstrated 45% over the same number of cycles. A major disadvantage of this organic cathode system in terms of energy density was the average discharge potential of 2.3 V, as compared to 3.6 V in our PEO_{20}-$KTFSI_1$ cell presented herein.

Due to a lack of comparison to other potassium cells based on solid electrolytes, we herein compare our electrochemical results with the study of Mindemark et al.,[66] who presented a solid-state sodium battery with a polymer electrolyte based on poly(trimethylene carbonate) (PTMC)-NaTFSI. The sodium cell composed of a Na-metal negative and a PBA-based $Na_2Fe[Fe(CN)_6]$ positive electrode was cycled at 60 °C. The experimental setup was quite comparable to the K-cells presented herein, although the demands to chemical stability are higher in the K-based systems since potassium metal is more reactive, and the average electrode potential of the K-PBA electrode is slightly higher than that of Na-PBA.[61] The authors demonstrated eight cycles at C/10 with a capacity retention of 94%, which would normally lead to a rapid capacity decay in conventional LE-cells at elevated temperatures. In another study, Mindemark and co-workers[67] demonstrated a sodium metal cell with the Na-PBA positive electrode enabled by the PTMC-NaFSI SPE, possessing superior ionic conductivities, particularly under room temperature conditions, thus allowing the cycling rate of C/5 at temperature as low as 40 °C. Under these conditions, the cell showed a capacity retention of 94% over 80 cycles. In general, these results are in good agreement with our observations on the PEO_{20}-$KTFSI_1$ system that demonstrated improved capacity retention and CE as compared to a corresponding LE-based system (Figure 4c,d). Overall, it should be highlighted that the reactivity of the alkali metal counter electrode plays a vital role for the interfacial resistance and capacity retention, which is often not given in a regular LE. However, to decrease the evaluated temperature, which generally triggers irreversible side reactions during cycling, the ionic conductivity along with the mechanical stability of K-based SPEs should be further enhanced through advanced materials design, for example, block-copolymer structures[32] or addition of ceramic fillers (such as Al_2O_3, SiO_2, TiO_2, and so forth)[68−71] that provide boosted cation transport along with structural integrity.

4. CONCLUSIONS

PEO-KTFSI with different KTFSI salt concentrations was investigated for its use as the SPE in potassium batteries. Both PEO and KTFSI have so far received little to no attention as K^+-conducting electrolytes, despite their relevance in related cell chemistries.

The best compromise between ionic conductivity and mechanical stability over the relevant operation temperature range between room temperature and 65 °C was obtained from the PEO-KTFSI blend with the lowest salt content, that is, an EO:KTFSI ratio of 20:1 ("PEO_{20}-$KTFSI_1$"). Although blends with higher EO:KTFSI ratios, that is, between 12:1 and 16:1 ("PEO_{12}-$KTFSI_1$" and "PEO_{16}-$KTFSI_1$"), yielded mostly amorphous materials with the highest ionic conductivities of up to $\approx 2 \times 10^{-5}$ to 4×10^{-5} S/cm at 25 °C, they had to be discarded for SPE applications owing to their poor rheological properties unsuitable to act as a separator. Blends with higher salt contents, i.e., EO:KTFSI 8:1 and 4:1 ("PEO_8-$KTFSI_1$" and "PEO_4-$KTFSI_1$"), demonstrated a notable drop in ionic conductivities ($\approx 2 \times 10^{-7}$ to 4×10^{-8} S/cm at 25 °C) yet providing the desired mechanical strength in the operating temperature range.

The SPEs were integrated in solid-state potassium batteries comprising a $K_2Fe[Fe(CN)_6]$ positive electrode and a K-metal with an average voltage of 3.6 V, making the results directly comparable to the state-of-the-art full cell configurations employing LEs.[4]

The cell employing the PEO_{20}-$KTFSI_1$ electrolyte that achieved a practical discharge capacity of 108.1 mAh g^{-1} was about 5% lower than the initial discharge capacity of a corresponding LE-cell. However, the SPE-cell showed significantly improved capacity retention (24% higher over 50 cycles) and CE (98 vs 83% for the LE-cell in the 50th cycle) owing to the better electrochemical stability of the polymer electrolyte. Because of their poor ionic conductivity, even at elevated temperatures, the SPE formulations PEO_4-$KTFSI_1$ and PEO_8-$KTFSI_1$ showed poor performance as a result of strong polarization effects.

In addition, the PEO_{20}-$KTFSI_1$ blend was subjected to a rate capability test, showing that the cycling rate can be further increased to up to C/15 without compromises in terms of polarization effect or capacity loss.

In conclusion, the PEO_{20}-$KTFSI_1$ blend offered the best trade-off between ion transport and mechanical properties and provided promising electrochemical results with respect to cycle life and capacity retention.

■ ASSOCIATED CONTENT

Supporting Information

The Supporting Information is available free of charge at https://pubs.acs.org/doi/10.1021/acsapm.2c00014.

Exemplary EIS spectra of the ionic conductivity measurements in section 2.3; XRD patterns of KTFSI,

https://doi.org/10.1021/acsapm.2c00014
ACS Appl. Polym. Mater. XXXX, XXX, XXX−XXX

PEO, and PEO-KTFSI polymer electrolyte; XRD pattern of $K_2Fe[Fe(CN)_6]$; and voltage profiles for selected cycles to the cycling data presented in Figure 4 (section 2.4) (PDF)

AUTHOR INFORMATION

Corresponding Author

Fabian Jeschull − *Institute for Applied Materials - Energy Storage Systems (IAM-ESS), Karlsruhe Institute of Technology (KIT), 76344 Eggenstein-Leopoldshafen, Germany;* orcid.org/0000-0002-5927-1978; Email: fabian.jeschull@kit.edu

Authors

Anna D. Khudyshkina − *Institute for Applied Materials - Energy Storage Systems (IAM-ESS), Karlsruhe Institute of Technology (KIT), 76344 Eggenstein-Leopoldshafen, Germany;* orcid.org/0000-0003-4532-8985

Polina A. Morozova − *Center for Energy Science and Technology, Skolkovo Institute of Science and Technology, 143025 Moscow, Russian Federation*

Andreas J. Butzelaar − *Institute for Chemical Technology and Polymer Chemistry (ITCP), Karlsruhe Institute of Technology (KIT), 76131 Karlsruhe, Germany;* orcid.org/0000-0002-0843-2719

Maxi Hoffmann − *Institute for Chemical Technology and Polymer Chemistry (ITCP), Karlsruhe Institute of Technology (KIT), 76131 Karlsruhe, Germany;* orcid.org/0000-0001-5100-8481

Manfred Wilhelm − *Institute for Chemical Technology and Polymer Chemistry (ITCP), Karlsruhe Institute of Technology (KIT), 76131 Karlsruhe, Germany;* orcid.org/0000-0003-2105-6946

Patrick Theato − *Institute for Chemical Technology and Polymer Chemistry (ITCP), Karlsruhe Institute of Technology (KIT), 76131 Karlsruhe, Germany; Soft Matter Synthesis Laboratory - Institute for Biological Interfaces III (IBG-3), Karlsruhe Institute of Technology (KIT), 76344 Eggenstein-Leopoldshafen, Germany;* orcid.org/0000-0002-4562-9254

Stanislav S. Fedotov − *Center for Energy Science and Technology, Skolkovo Institute of Science and Technology, 143025 Moscow, Russian Federation*

Complete contact information is available at: https://pubs.acs.org/10.1021/acsapm.2c00014

Notes

The authors declare no competing financial interest.

The data that support the findings of this study are openly available in Zenodo online repository at 10.5281/zenodo.5682615, reference number.[72]

ACKNOWLEDGMENTS

Financial support from the German Federal Ministry of Education and Research (BMBF) within "FestBatt" (13XP0175C) is gratefully acknowledged. The authors acknowledge financial support via the Helmholtz Association. P.A.M and S.S.F acknowledge support from Russian Foundation for Basic Research (grant #21-53-12039). This work contributes to the research performed within the Post Lithium Storage Cluster of Excellence (POLiS), funded by the Deutsche Forschungsgemeinschaft (DFG, German Research Foundation) under Germany's Excellence Strategy—EXC 2154—Project number 390874152, as well as to the research performed at the Center for Electrochemical Energy Storage Ulm-Karlsruhe (CELEST). Furthermore, the authors gratefully acknowledge the German Research Foundation for financial support (grant #448719339) within the framework of the bilateral German-Russian research projects (RFBR-DFG Cooperation).

REFERENCES

(1) V, A.; John, B.; TD, M. Potassium-Ion Batteries: Key to Future Large-Scale Energy Storage? *ACS Appl. Energy Mater.* **2020**, *3*, 9478−9492.

(2) Min, X.; Xiao, J.; Fang, M.; Wang, W.; Zhao, Y.; Liu, Y.; Abdelkader, A. M.; Xi, K.; Kumar, R. V.; Huang, Z. Potassium-Ion Batteries: Outlook on Present and Future Technologies. *Energy Environ. Sci.* **2021**, *14*, 2186−2243.

(3) Rajagopalan, R.; Tang, Y.; Ji, X.; Jia, C.; Wang, H. Advancements and Challenges in Potassium Ion Batteries: A Comprehensive Review. *Adv. Funct. Mater.* **2020**, *30*, No. 1909486.

(4) Bie, X.; Kubota, K.; Hosaka, T.; Chihara, K.; Komaba, S. A Novel K-Ion Battery: Hexacyanoferrate(II)/Graphite Cell. *J. Mater. Chem. A* **2017**, *5*, 4325−4330.

(5) Fedotov, S. S.; Khasanova, N. R.; Samarin, A. S.; Drozhzhin, O. A.; Batuk, D.; Karakulina, O. M.; Hadermann, J.; Abakumov, A. M.; Antipov, E. V. AVPO4F (A = Li, K): A 4 v Cathode Material for High-Power Rechargeable Batteries. *Chem. Mater.* **2016**, *28*, 411−415.

(6) Xu, Y. S.; Duan, S. Y.; Sun, Y. G.; Bin, D. S.; Tao, X.; Zhang, D.; Liu, Y.; Cao, A. M.; Wan, L. J. Recent Developments in Electrode Materials for Potassium-Ion Batteries. *J. Mater. Chem. A* **2019**, *7*, 4334−4352.

(7) Ahmed, S. M.; Suo, G.; Wang, W. A.; Xi, K.; Iqbal, S. Improvement in Potassium Ion Batteries Electrodes: Recent Developments and Efficient Approaches. *J. Energy Chem.* **2021**, *62*, 307−337.

(8) Morozova, P. A.; Trussov, I. A.; Rupasov, D. P.; Nikitina, V. A.; Abakumov, A. M.; Fedotov, S. S. Exploring the Role of Crystal Water in Potassium Manganese Hexacyanoferrate as a Cathode Material for Potassium-Ion Batteries. *Crystals* **2021**, *11*, 895.

(9) Zhu, Y. H.; Yin, Y.; Yang, X.; Sun, T.; Wang, S.; Jiang, Y. S.; Yan, J. M.; Zhang, X. B. Transformation of Rusty Stainless-Steel Meshes into Stable, Low-Cost, and Binder-Free Cathodes for High-Performance Potassium-Ion Batteries. *Angew. Chem. Int. Ed.* **2017**, *56*, 7881−7885.

(10) Fei, H.; Liu, Y.; An, Y.; Xu, X.; Zeng, G.; Tian, Y.; Ci, L.; Xi, B.; Xiong, S.; Feng, J. Stable All-Solid-State Potassium Battery Operating at Room Temperature with a Composite Polymer Electrolyte and a Sustainable Organic Cathode. *J. Power Sources* **2018**, *399*, 294−298.

(11) Kim, H.; Tian, Y.; Ceder, G. Origin of Capacity Degradation of High-Voltage KVPO 4 F Cathode. *J. Electrochem. Soc.* **2020**, *167*, 110555.

(12) Jeschull, F.; Maibach, J. Inactive Materials Matter: How Binder Amounts Affect the Cycle Life of Graphite Electrodes in Potassium-Ion Batteries. *Electrochem. Commun.* **2020**, *121*, 106874.

(13) Komaba, S.; Hasegawa, T.; Dahbi, M.; Kubota, K. Potassium Intercalation into Graphite to Realize High-Voltage/High-Power Potassium-Ion Batteries and Potassium-Ion Capacitors. *Electrochem. Commun.* **2015**, *60*, 172−175.

(14) Madec, L.; Gabaudan, V.; Gachot, G.; Stievano, L.; Monconduit, L.; Martinez, H. Paving the Way for K-Ion Batteries: Role of Electrolyte Reactivity through the Example of Sb-Based Electrodes. *ACS Appl. Mater. Interfaces* **2018**, *10*, 34116−34122.

(15) Wang, H.; Zhai, D.; Kang, F. Solid Electrolyte Interphase (SEI) in Potassium Ion Batteries. *Energy Environ. Sci.* **2020**, *13*, 4583−4608.

(16) Boaretto, N.; Meabe, L.; Martinez-Ibañez, M.; Armand, M.; Zhang, H. Review—Polymer Electrolytes for Rechargeable Batteries: From Nanocomposite to Nanohybrid. *J. Electrochem. Soc.* **2020**, *167*, No. 070524.

(17) Yue, L.; Ma, J.; Zhang, J.; Zhao, J.; Dong, S.; Liu, Z.; Cui, G.; Chen, L. All Solid-State Polymer Electrolytes for High-Performance Lithium Ion Batteries. *Energy Storage Mater.* **2016**, *5*, 139−164.
(18) Yao, P.; Yu, H.; Ding, Z.; Liu, Y.; Lu, J.; Lavorgna, M.; Wu, J.; Liu, X. Review on Polymer-Based Composite Electrolytes for Lithium Batteries. *Front. Chem.* **2019**, *7*, 522.
(19) Mindemark, J.; Lacey, M. J.; Bowden, T.; Brandell, D. Beyond PEO—Alternative Host Materials for Li+-Conducting Solid Polymer Electrolytes. *Prog. Polym. Sci.* **2018**, *81*, 114−143.
(20) Fei, H.; Liu, Y.; An, Y.; Xu, X.; Zhang, J.; Xi, B.; Xiong, S.; Feng, J. Safe All-Solid-State Potassium Batteries with Three Dimentional, Flexible and Binder-Free Metal Sulfide Array Electrode. *J. Power Sources* **2019**, *433*, No. 226697.
(21) Homann, G.; Stolz, L.; Nair, J.; Laskovic, I. C.; Winter, M.; Kasnatscheew, J. Poly(Ethylene Oxide)-Based Electrolyte for Solid-State-Lithium-Batteries with High Voltage Positive Electrodes: Evaluating the Role of Electrolyte Oxidation in Rapid Cell Failure. *Sci. Rep.* **2020**, *10*, 1−9.
(22) Jiang, Y.; Yan, X.; Ma, Z.; Mei, P.; Xiao, W.; You, Q.; Zhang, Y. Development of the PEO Based Solid Polymer Electrolytes for All-Solid State Lithium Ion Batteries. *Polymers* **2018**, *10*, 1237.
(23) Oteo, U.; Martinez-Ibañez, M.; Aldalur, I.; Sanchez-Diez, E.; Carrasco, J.; Armand, M.; Zhang, H. Improvement of the Cationic Transport in Polymer Electrolytes with (Difluoromethanesulfonyl)-(Trifluoromethanesulfonyl)Imide Salts. *ChemElectroChem* **2019**, *6*, 1019−1022.
(24) Perrier, M.; Besner, S.; Paquette, C.; Vallée, A.; Lascaud, S.; Prud'homme, J. Mixed-alkali effect and short-range interactions in amorphous poly(ethylene oxide) electrolytes. *Electrochim. Acta* **1995**, *40*, 2123−2129.
(25) Yin, H.; Han, C.; Liu, Q.; Wu, F.; Zhang, F.; Tang, Y. Recent Advances and Perspectives on the Polymer Electrolytes for Sodium/Potassium-Ion Batteries. *Small* **2021**, *17*, No. 2006627.
(26) Zhao, S.; Guo, Z.; Yan, K.; Guo, X.; Wan, S.; He, F.; Sun, B.; Wang, G. The Rise of Prussian Blue Analogs: Challenges and Opportunities for High-Performance Cathode Materials in Potassium-Ion Batteries. *Small Struct.* **2021**, *2*, No. 2000054.
(27) Wang, B.; Han, Y.; Wang, X.; Bahlawane, N.; Pan, H.; Yan, M.; Jiang, Y. Prussian Blue Analogs for Rechargeable Batteries. *iScience* **2018**, *3*, 110−133.
(28) Jeschull, F.; Trabesinger, S. Fast-Charge Limitations for Graphite Anodes with Si as Capacity-Enhancing Additive. *Batter. Supercaps* **2021**, *4*, 131−139.
(29) Kim, Y. W.; Lee, W.; Choi, B. K. Relation between Glass Transition and Melting of PEO-Salt Complexes. *Electrochim. Acta* **2000**, *45*, 1473−1477.
(30) He, R.; Kyu, T. Effect of Plasticization on Ionic Conductivity Enhancement in Relation to Glass Transition Temperature of Crosslinked Polymer Electrolyte Membranes. *Macromolecules* **2016**, *49*, 5637−5648.
(31) Brooks, D. J.; Merinov, B. V.; Goddard, W. A.; Kozinsky, B.; Mailoa, J. Atomistic Description of Ionic Diffusion in PEO−LiTFSI: Effect of Temperature, Molecular Weight, and Ionic Concentration. *Macromolecules* **2018**, *51*, 8987−8995.
(32) Butzelaar, A. J.; Röring, P.; Mach, T. P.; Hoffmann, M.; Jeschull, F.; Wilhelm, M.; Winter, M.; Brunklaus, G.; Théato, P. Styrene-Based Poly(Ethylene Oxide) Side-Chain Block Copolymers as Solid Polymer Electrolytes for High-Voltage Lithium-Metal Batteries. *ACS Appl. Mater. Interfaces* **2021**, *13*, 39257−39270.
(33) Stolz, L.; Röser, S.; Homann, G.; Winter, M.; Kasnatscheew, J. Pragmatic Approaches to Correlate between the Physicochemical Properties of a Linear Poly(Ethylene Oxide)-Based Solid Polymer Electrolyte and the Performance in a High-Voltage Li-Metal Battery. *J. Phys. Chem. C* **2021**, *125*, 18089−18097.
(34) Saeed, R. M.; Schlegel, J. P.; Castano, C.; Sawafta, R. Uncertainty of Thermal Characterization of Phase Change Material by Differential Scanning Calorimetry Analysis. *Int. J. Eng. Res. Technol.* **2016**, *5*, 405−412.
(35) Le Nest, J. F.; Gandini, A.; Cheradame, H.; Cohen-Addad, J. P. Influence of LiCLO4on the Properties of Polyether Networks: Specific Volume and Glass Transition Temperature. *Macromolecules* **1988**, *21*, 1117−1120.
(36) Mao, G.; Perea, R. F.; Howells, W. S.; Price, D. L.; Saboungi, M.-L. Relaxation in Polymer Electrolytes on the Nanosecond Timescale. *Nature* **2000**, *405*, 163−165.
(37) Butzelaar, A. J.; Liu, K. L.; Röring, P.; Brunklaus, G.; Winter, M.; Theato, P. A Systematic Study of Vinyl Ether-Based Poly-(Ethylene Oxide) Side-Chain Polymer Electrolytes. *ACS Appl. Polym. Mater.* **2021**, *3*, 1573−1582.
(38) Shin, J. Ionic Liquids to the Rescue? Overcoming the Ionic Conductivity Limitations of Polymer Electrolytes. *Electrochem. Commun.* **2003**, *5*, 1016−1020.
(39) Dreezen, G.; Koch, M. H. J.; Reynaers, H.; Groeninckx, G. Miscible Binary Blends of Poly(Ethylene Oxide) and an Amorphous Aromatic Polyamide (Aramide 34I): Crystallization, Melting Behavior and Semi-Crystalline Morphology. *Polymer* **1999**, *40*, 6451−6463.
(40) Lascaud, S.; Perrier, M.; Vallee, A.; Besner, S.; Prud'homme, J.; Armand, M. Phase Diagrams and Conductivity Behavior of Poly-(Ethylene Oxide)-Molten Salt Rubbery Electrolytes. *Macromolecules* **1994**, *27*, 7469−7477.
(41) Angell, C. A.; Liu, C.; Sanchez, E. Rubbery Solid Electrolytes with Dominant Cationic Transport and High Ambient Conductivity. *Nature* **1993**, *362*, 137−139.
(42) Yi, C.; Liu, W.; Li, L.; Dong, H.; Liu, J. Polymer-in-Salt Solid Electrolytes for Lithium-Ion Batteries. *Funct. Mater. Lett.* **2019**, *12*, No. 1930006.
(43) Yang, S.; Liu, Z.; Liu, Y.; Jiao, Y. Effect of Molecular Weight on Conformational Changes of PEO: An Infrared Spectroscopic Analysis. *J. Mater. Sci.* **2015**, *50*, 1544.
(44) Lisowski, M. S.; Liu, Q.; Cho, J.; Runt, J.; Yeh, F.; Hsiao, B. S. Crystallization Behavior of Poly(Ethylene Oxide) and Its Blends Using Time-Resolved Wide-and Small-Angle X-Ray Scattering. *Macromolecules* **2000**, *33*, 4842.
(45) Marzantowicz, M.; Dygas, J. R.; Krok, F.; Nowiński, J. L.; Tomaszewska, A.; Florjańczyk, Z.; Zygadło-Monikowska, E. Crystalline Phases, Morphology and Conductivity of PEO:LiTFSI Electrolytes in the Eutectic Region. *J. Power Sources* **2006**, *159*, 420−430.
(46) Rowe, M. C.; Brewer, B. J. AMORPH: A Statistical Program for Characterizing Amorphous Materials by X-Ray Diffraction. *Comput. Geosci.* **2018**, *120*, 21−31.
(47) Lopez, J.; Mackanic, D. G.; Cui, Y.; Bao, Z. Designing Polymers for Advanced Battery Chemistries. *Nat. Rev. Mater.* **2019**, *4*, 312−330.
(48) Zhao, Q.; Liu, X.; Stalin, S.; Archer, L. In-Built Polymer-in-Solvent and Solvent-in-Polymer Electrolytes for High-Voltage Lithium Metal Batteries. *Cell Rep. Phys. Sci.* **2020**, *1*, No. 100146.
(49) Brandell, D.; Mindemark, J.; Hernández, G. *Polymer-Based Solid State Batteries*; De Gruyter: Boston, Berlin 2021.
(50) Hashim, N. H. A. M.; Subban, R. H. Y. Studies on Conductivity, Structural and Thermal Properties of PEO-LiTFSI Polymer Electrolytes Doped with EMImTFSI Ionic Liquid. *J. Chem. Phys.* **2031**, *143*, 24904.
(51) Devaux, D.; Bouchet, R.; Glé, D.; Denoyel, R. Mechanism of Ion Transport in PEO/LiTFSI Complexes: Effect of Temperature, Molecular Weight and End Groups. *Solid State Ionics* **2012**, *227*, 119−127.
(52) Maurel, A.; Armand, M.; Grugeon, S.; Fleutot, B.; Davoisne, C.; Tortajada, H.; Courty, M.; Panier, S.; Dupont, L. Poly(Ethylene Oxide)−LiTFSI Solid Polymer Electrolyte Filaments for Fused Deposition Modeling Three-Dimensional Printing. *J. Electrochem. Soc.* **2020**, *167*, No. 070536.
(53) Aziz, S. B.; Woo, T. J.; Kadir, M. F. Z.; Ahmed, H. M. A Conceptual Review on Polymer Electrolytes and Ion Transport Models. *J. Sci. Adv. Mater. Devices* **2018**, 3, 1−17.
(54) Siva Kumar, J.; Subrahmanyam, A. R.; Jaipal Reddy, M.; Subba Rao, U. V. Preparation and Study of Properties of Polymer Electrolyte System (PEO+NaClO3). *Mater. Lett.* **2006**, *60*, 3346−3349.

https://doi.org/10.1021/acsapm.2c00014
ACS Appl. Polym. Mater. XXXX, XXX, XXX−XXX

(55) Jaipal Reddy, M.; Sreekanth, T.; Subba Rao, U. V. Study of the Plasticizer Effect on a (PEO + NaYF4) Polymer Electrolyte and Its Use in an Electrochemical Cell. *Solid State Ionics* **1999**, *126*, 55−63.
(56) Gadjourova, Z.; Andreev, Y. G.; Tunstall, D. P.; Bruce, P. G. Ionic Conductivity in Crystalline Polymer Electrolytes. *Nature* **2001**, *412*, 520−523.
(57) Stoeva, Z.; Martin-Litas, I.; Staunton, E.; Andreev, Y. G.; Bruce, P. G. Ionic Conductivity in the Crystalline Polymer Electrolytes PEO6:LiXF6, X = P, As, Sb. *J. Am. Chem. Soc.* **2003**, *125*, 4619−4626.
(58) Kim, H.; Ji, H.; Wang, J.; Ceder, G. Next-Generation Cathode Materials for Non-Aqueous Potassium-Ion Batteries. *Trends Chem.* **2019**, *1*, 682−692.
(59) Allgayer, F.; Maibach, J.; Jeschull, F. Comparing the Solid Electrolyte Interphases on Graphite Electrodes in K and Li Half Cells. *ACS Appl. Energy Mater.* **2022**, *5*, 1136−1148.
(60) Sahore, R.; Yang, G.; Chen, X. C.; Tsai, W.-Y.; Li, J.; Dudney, N. J.; Westover, A. A Bilayer Electrolyte Design to Enable High-Areal-Capacity Composite Cathodes in Polymer Electrolytes Based Solid-State Lithium Metal Batteries. *ACS Appl. Energy Mater.* **2022**, *5*, 1409.
(61) Kubota, K.; Dahbi, M.; Hosaka, T.; Kumakura, S.; Komaba, S. Towards K-Ion and Na-Ion Batteries as "Beyond Li-Ion.". *Chem. Rec.* **2018**, *18*, 459−479.
(62) Notten, P. H. L.; Veld, J. H. G. O. H.; Van Beek, J. R. G. Boostcharging Li-Ion Batteries: A Challenging New Charging Concept. *J. Power Sources* **2005**, *145*, 89−94.
(63) Amietszajew, T.; McTurk, E.; Fleming, J.; Bhagat, R. Understanding the Limits of Rapid Charging Using Instrumented Commercial 18650 High-Energy Li-Ion Cells. *Electrochim. Acta* **2018**, *263*, 346−352.
(64) Stolz, L.; Homann, G.; Winter, M.; Kasnatscheew, J. Kinetical Threshold Limits in Solid-State Lithium Batteries: Data on Practical Relevance of Sand Equation. *Data Brief* **2021**, *34*, No. 106688.
(65) Stolz, L.; Homann, G.; Winter, M.; Kasnatscheew, J. The Sand Equation and Its Enormous Practical Relevance for Solid-State Lithium Metal Batteries. *Mater. Today* **2021**, *44*, 9−14.
(66) Mindemark, J.; Mogensen, R.; Smith, M. J.; Silva, M. M.; Brandell, D. Polycarbonates as Alternative Electrolyte Host Materials for Solid-State Sodium Batteries. *Electrochem. Commun.* **2017**, *77*, 58−61.
(67) Sångeland, C.; Mogensen, R.; Brandell, D.; Mindemark, J. Stable Cycling of Sodium Metal All-Solid-State Batteries with Polycarbonate-Based Polymer Electrolytes. *ACS Appl. Polym. Mater.* **2019**, *1*, 825−832.
(68) Croce, F.; Persi, L. L.; Scrosati, B.; Serraino-Fiory, F.; Plichta, E.; Hendrickson, M. A. Role of the Ceramic Fillers in Enhancing the Transport Properties of Composite Polymer Electrolytes. *Electrochim. Acta* **2001**, *46*, 2457−2461.
(69) Feng, J.; Wang, L.; Chen, Y.; Wang, P.; Zhang, H.; He, X. PEO Based Polymer-Ceramic Hybrid Solid Electrolytes: A Review. *Nano Converg.* **2021**, *8*, 1−12.
(70) Song, Y. W.; Heo, K.; Lee, J.; Hwang, D.; Kim, M. Y.; Kim, S. J.; Kim, J.; Lim, J. Lithium-Ion Transport in Inorganic Active Fillers Used in PEO-Based Composite Solid Electrolyte Sheets. *RSC Adv.* **2021**, *11*, 31855−31864.
(71) Hoang Huy, V. P.; So, S.; Hur, J. Inorganic Fillers in Composite Gel Polymer Electrolytes for High-Performance Lithium and Non-Lithium Polymer Batteries. *Nanomaterials* **2021**, *11*, 614.
(72) Khudyshkina, A. D.; Morozova, P. A.; Butzelaar, A. J.; Hoffmann, M.; Wilhelm, M.; Theato, P.; Fedotov, S. S.; Jeschull, F. Datasets to Poly(Ethylene Oxide)-Based Electrolytes for Solid-State Potassium Metal Batteries with Prussian Blue Positive Electrode. *Zenodo Online Repos.* **2021**, DOI: 10.5281/zenodo.5682615.

https://doi.org/10.1021/acsapm.2c00014
ACS Appl. Polym. Mater. XXXX, XXX, XXX−XXX